Available online at www.sciencedirect.com
ScienceDirect
International Journal of Solids and Structures 45 (2008) 3644–3659
INTERNATIONAL JOURNAL OF SOLIDS AND STRUCTURES
www.elsevier.com/locate/ijsolstr

Asymptotic crack-tip fields for dynamic crack growth in compressive power-law hardening materials

Xian-Kui Zhu [a,*], Keh-Chih Hwang [b]

[a] Battelle Memorial Institute, 505 King Avenue, Columbus, OH 43201, USA
[b] Department of Engineering Mechanics, Tsinghua University, Beijing 100084, China

Received 21 May 2007
Available online 6 September 2007

Abstract

The effect of material compressibility on the stress and strain fields for a mode-I crack propagating steadily in a power-law hardening material is investigated under plane strain conditions. The plastic deformation of materials is characterized by the J_2 flow theory within the framework of isotropic hardening and infinitesimal displacement gradient. The asymptotic solutions developed by the present authors [Zhu, X.K., Hwang K.C., 2002. Dynamic crack-tip field for tensile cracks propagating in power-law hardening materials. International Journal of Fracture 115, 323–342] for incompressible hardening materials are extended in this work to the compressible hardening materials. The results show that all stresses, strains, and particle velocities in the asymptotic fields are fully continuous and bounded without elastic unloading near the dynamic crack tip. The stress field contains two free parameters σ_{eq0} and s_{330} that cannot be determined in the asymptotic analysis, and can be determined from the full-field solutions. For the given values of σ_{eq0} and s_{330}, all field quantities around the crack tip are determined through numerical integration, and then the effects of the hardening exponent n, the Poisson ratio v, and the crack growth speed M on the asymptotic fields are studied. The approximate behaviors of the proposed solutions are discussed in the limit of $v \to 0.5$ or $n \to \infty$.

Keywords: Asymptotic solution; Crack-tip field; Mode-I crack; Dynamic crack growth; Power-law hardening material; Compressibility; Plane strain condition

1. Introduction

Deformation and failure of dynamic cracks have been investigated for years due to its significant importance in engineering. A monograph of Freund (1998) systematically elaborated the general concepts, methods, and results for dynamic cracks propagating in both elastic and elastic–plastic materials. Rosakis and Ravichandran (2000) reviewed the current research status of dynamic failure mechanics. In general, two kinds of dynamic cracks are categorized. One is the dynamic cracks caused impact loads that are primarily studied in dynamic crack initiation (Wall, 2002). The other is dynamic cracks propagating steadily that are primarily

* Corresponding author. Tel.: +1 614 424 4387; fax: +1 614 424 4587.
E-mail address: zhux@battelle.org (X.-K. Zhu).

0020-7683/$ - see front matter © 2007 Elsevier Ltd. All rights reserved.
doi:10.1016/j.ijsolstr.2007.07.019

investigated in the analysis of asymptotic fields (Zhang et al., 2003). The present work will focus on mode-I dynamic cracks growing steadily in power-law hardening materials under the plane strain condition.

For elastic dynamic cracks, the solutions of crack-tip fields are accepted commonly. For elastic–plastic dynamic cracks, however, there are different asymptotic and numerical solutions, and the broad agreements among them could not be found due to the extremely complexity. For elastic–perfectly plastic materials, Gao and Nemat-Nasser (1983a) and Gao (1985) proposed the asymptotic solutions that contain strong discontinuities, in which the stresses are bounded, and the strains are logarithmically singular at the crack tip. For power-law hardening materials, Gao and Nemat-Nasser (1983b) and Zhu and Hwang (1996) proposed dynamic near-tip fields with discontinuous and logarithmically singular stresses and strains. However, Leighton et al. (1987) demonstrated that the principle of the maximum plastic work prohibits the existence of any dynamic discontinuities in stress, strain, and velocity fields for an incompressible elastic–perfectly plastic material, and successfully constructed a unique asymptotic crack-tip field with fully continuous and bounded stresses, strains, and particle velocities for the material. Similarly using the maximum plastic work principle, Drugan and Shen (1987), Zhu (1995), and Zhang et al. (1997) confirmed that dynamic strong discontinuities are not allowed for any field quantities at the dynamic crack tip for non-hardening and hardening materials. Accordingly, Zhang et al. (1997) extended the continuous solutions of Leighton et al. (1987) to the compressible elastic–perfectly plastic material, and obtained an asymptotic crack-tip field with continuous and bounded stresses and strains. Zhu and Hwang (2002) further extended these continuous solutions to the incompressible power-law hardening materials after a detailed review of the asymptotic solutions for elastic–plastic dynamic crack growth.

Lam and Freund (1985) could be the pioneers who reported numerical solutions of dynamic mode-I crack growth using finite element analysis (FEA) for elastic–perfectly plastic materials. Xu and Saigal (1999) obtained numerical results of the dynamic crack growth for linear and power-law hardening materials using the Element Free Galerkin (EFG) method. The EFG solutions agree well with the FEA results as the material hardening vanishes, and both numerical results indicated that the stresses and strains are continuous near the crack tip. On the other hand, Varias and Shih (1994) presented a different FEA results that exhibit sizable jumps in both stresses and strains at $\theta \approx 90^\circ$ for elastic–plastic materials with and without strain hardening. Due to the reasons introduced above, a physically realizable solution should be continuous near the crack tip, and thus the discontinuous solutions must be ruled out. Nevertheless, all numerical solutions showed the occurrence of elastic unloading near the crack surfaces that were not observed in available asymptotic solutions.

The present paper extends the companion work in Zhu and Hwang (2002) for incompressible power-law hardening material to the compressible power-law hardening materials, and constructs continuous stress and deformation fields for the steady dynamic crack growth. The detailed discussions are performed for the effects of the hardening exponent n, the Poisson ratio v, and the crack growth speed M on the asymptotic fields, and for the approximate behaviors of the proposed solutions in the limit of $v \to 0.5$ or $n \to \infty$.

2. Basic equations and boundary conditions

2.1. Basic equations

Consider a mode-I dynamic crack propagating steadily at speed V in a compressible power-law hardening material under plane strain conditions. The elastic–plastic responses of materials are characterized by the J_2 flow theory within the framework of isotropic hardening and infinitesimal displacement gradient. Both the rectangular coordinates (x_1, x_2) and the polar coordinates (r, θ) are introduced with their common origin fixed at the crack tip and the edge line $\theta = 0$ aligned to the x_1 direction. The two coordinate systems translate with the crack tip that moves steadily in the x_1 direction at the speed V.

In reference to the rectangular components of the Cauchy stress tensor and the particle velocity vector, $\sigma_{\alpha\beta}$ and v_α, the equations of momentum balance are expressed as:

$$\sigma_{\alpha\beta,\beta} = \rho \dot{\mathrm{v}}_\alpha \tag{1}$$

where ρ is the material mass density, the comma in the subscript denotes the differentiation with respect to the coordinate x_β and the superimposed dot denotes a material time derivative. In this paper, the repeated indices

follow the usual summation convention. The Latin indices range from 1 to 3, whereas the Greek indices range only from 1 to 2.

For the infinitesimal deformation, in terms of the particle velocity v_α and the rectangular components of the strain tensor $\varepsilon_{\alpha\beta}$, the components of the small strain rate tensor have the form of:

$$\dot{\varepsilon}_{\alpha\beta} = \frac{1}{2}(v_{\alpha,\beta} + v_{\beta,\alpha}) \tag{2}$$

According to the J_2 flow theory of plasticity, the elastic–plastic deformation of materials obeys the Prandtl–Reuss constitutive rule:

$$\dot{\varepsilon}_{ij} = \frac{1}{2\mu}\left(\dot{s}_{ij} + \frac{1-2\nu}{3(1+\nu)}\dot{\sigma}_{kk}\delta_{ij}\right) + \lambda s_{ij} \tag{3}$$

where μ is the elastic shear modulus, ν is the Poisson's ratio, δ_{ij} is the Kronecker delta, $s_{ij} = \sigma_{ij} - \sigma_{kk}\delta_{ij}/3$ are the rectangular components of deviatoric stress tensor, and λ is the non-negative plastic flow factor. As the material hardens, the plastic strain follows the power-law stress–strain relation in uniaxial tension:

$$\varepsilon_p = c\left(\frac{\sigma}{\sigma_0}\right)^n \tag{4}$$

where σ and ε_p are the uniaxial stress and strain, respectively. c is a material constant, and $n > 1$ is the hardening exponent, σ_0 is the initial yield stress. From (4), using the normality rule of plastic deformation in the J_2 flow theory, one obtains the plastic flow factor:

$$\lambda = \frac{3nc}{2\sigma_0}\left(\frac{\sigma_{\mathrm{eq}}}{\sigma_0}\right)^{n-2}\frac{\dot{\sigma}_{\mathrm{eq}}}{\sigma_0} \tag{5}$$

where σ_{eq} is the Mises equivalent stress and defined by $\sigma_{\mathrm{eq}} = (3/2 s_{ij}s_{ij})^{1/2}$.

2.2. Plane strain conditions

Under plane strain conditions, one has $\varepsilon_{33} = 0$. From (3) and in reference to the stress components, this plane strain condition becomes:

$$\dot{s}_{33} + \frac{1-2\nu}{2(1+\nu)}(\dot{\sigma}_{11} + \dot{\sigma}_{22} + \dot{s}_{33}) + 2\mu\lambda s_{33} = 0 \tag{6}$$

2.3. Boundary conditions

For the mode-I crack, the symmetric conditions are:

$$\sigma_{12}(r,0) = 0, \qquad v_2(r,0) = 0 \tag{7}$$

The traction-free conditions on crack faces require:

$$\sigma_{22}(r,\pm\pi) = 0, \qquad \sigma_{12}(r,\pm\pi) = 0 \tag{8}$$

2.4. Continuity conditions

Possible discontinuity of field quantities is an important problem in the study of dynamic crack-tip fields. As concluded in Zhu and Hwang (2002), the possibility of dynamic strong discontinuities for all field variables does not exist near the dynamic crack tip either for elastic–perfectly plastic materials or for power-law isotropic hardening materials, which can be mathematically expressed as:

$$[|\sigma_{ij}|] = 0, \quad [|\varepsilon_{ij}|] = 0, \quad [|v_i|] = 0 \tag{9}$$

The equations above infer that all components of stresses, strains, and particle velocities are continuous near the dynamic crack tip.

3. Asymptotic analyses and continuous solutions

3.1. Asymptotic governing equations

The present authors (Zhu and Hwang, 2002) successfully constructed a family of fully continuous dynamic crack-tip field for incompressible power-law hardening materials, by using an assumption that all components of stresses, strains, and particle velocities are bounded at the dynamic crack tip. Suppose this assumption is valid here, and all bounded field variables can be then expressed as functions of the polar coordinate θ only:

$$\begin{aligned}
&\sigma_{ij}(r,\theta) = \sigma_{ij}(\theta) + o(1)\\
&\varepsilon_{ij}(r,\theta) = \varepsilon_{ij}(\theta) + o(1)\\
&\mathrm{v}_i(r,\theta) = \mathrm{v}_i(\theta) + o(1)
\end{aligned} \tag{10}$$

where $o()$ is the symbol of infinitesimal order, and means that $o(1) \to 0$ as $r \to 0$. For steady-state crack growth, the material time derivative of any field variable, say g, is equivalent to the spatial derivative $-V\partial g/\partial x_1$. Since all field variables are functions of the polar coordinate θ only, the material time derivative of g is simplified as:

$$\dot{g} = -V\frac{\partial g}{\partial x_1} = \frac{V\sin\theta}{r}\frac{\partial g}{\partial \theta} \tag{11}$$

For the sake of brevity in mathematical analysis, we introduce four stress variables:

$$\begin{aligned}
&S_1(\theta) = s_{11}(\theta) + \frac{1}{2}s_{33}(\theta)\\
&S_2(\theta) = s_{12}(\theta)\\
&S_3(\theta) = s_{33}(\theta)\\
&\sigma_h = \frac{1}{2}(\sigma_{11} + \sigma_{22})
\end{aligned} \tag{12}$$

These four stress components together with the two velocity components $\mathrm{v}_1(\theta)$ and $\mathrm{v}_2(\theta)$ are chosen as six basic unknown variables for the problem considered. Accordingly, from (12), the components of stresses can be expressed by:

$$\begin{aligned}
&\sigma_{11}(\theta) = \sigma_h(\theta) + S_1(\theta)\\
&\sigma_{22}(\theta) = \sigma_h(\theta) - S_1(\theta)\\
&\sigma_{12}(\theta) = S_2(\theta)\\
&\sigma_{33}(\theta) = \sigma_h(\theta) + \frac{3}{2}S_3(\theta)
\end{aligned} \tag{13}$$

From (12) or (13), the Mises equivalent stress is expressed as:

$$\sigma_{\mathrm{eq}} = \sqrt{3}\left[S_1^2 + S_2^2 + \frac{3}{4}S_3^2\right]^{1/2} \tag{14}$$

In reference to the six basic unknown variables and using the steady-state condition (11), after a lengthy but straightforward manipulation through the substitution of (10), (13), and (14) into the momentum balance equation (1), the geometric relation (2), the constitutive equations (3) and (5), and the plane strain condition (6), one obtains the asymptotic governing equations of dynamic crack-tip fields as follows:

$$\begin{aligned} &C_{11}S_1'(\theta)+C_{12}S_2'(\theta)+C_{13}S_3'(\theta)=0\\ &C_{21}S_1'(\theta)+C_{22}S_2'(\theta)+C_{23}S_3'(\theta)=0\\ &C_{31}S_1'(\theta)+C_{32}S_2'(\theta)+C_{33}S_3'(\theta)=0 \end{aligned} \tag{15}$$

and

$$\begin{aligned} \sigma_h'(\theta) &= \frac{\cos 2\theta S_1'(\theta)+\sin 2\theta S_2'(\theta)+\frac{3\bar{v}}{2(1+v)}M^2\sin^2\theta S_3'(\theta)}{1-\frac{3\bar{v}}{1+v}M^2\sin^2\theta}\\ \lambda &= \frac{1}{2r\mu M^2\sin\theta[S_1^2(\theta)+S_2^2(\theta)]}\{(1-M^2\sin^2\theta)[S_1(\theta)S_1'(\theta)+S_2(\theta)S_2'(\theta)]\\ &\quad -\sigma_h'(\theta)[\cos 2\theta S_1(\theta)+\sin 2\theta S_2(\theta)]\}\\ v_1'(\theta) &= -\frac{V}{\mu M^2\sin\theta}[\sin\theta(S_1'(\theta)+\sigma_h'(\theta))-\cos\theta S_2'(\theta)]\\ v_2'(\theta) &= -\frac{V}{\mu M^2\sin\theta}[\cos\theta(S_1'(\theta)-\sigma_h'(\theta))+\sin\theta S_2'(\theta)] \end{aligned} \tag{16}$$

where the prime " $'$ " denotes the differentiation with respect to θ, i.e., $\mathrm{d}/\mathrm{d}\theta$. $\bar{v}=1/2-v$, $M=V/c_s$ is the Mach number for measuring the speed of crack propagation, and $c_s=\sqrt{\mu/\rho}$ is the elastic shear wave speed. In general, the Mach number M has the range: $0\leqslant M<1$ for dynamic crack growth (Freund, 1998). The coefficients $C_{11}\sim C_{33}$ in (15) are defined as:

$$\begin{aligned} C_{11} &= \cos 2\theta g-(1-M^2\sin^2\theta)\left(1-\frac{3\bar{v}}{1+v}M^2\sin^2\theta\right)S_2\\ C_{12} &= \sin 2\theta g+(1-M^2\sin^2\theta)\left(1-\frac{3\bar{v}}{1+v}M^2\sin^2\theta\right)S_1 \end{aligned} \tag{17a}$$

$$C_{13}=\frac{3\bar{v}}{2(1+v)}M^2\sin^2\theta g$$

$$\begin{aligned} C_{21} &= (1-M^2\sin^2\theta)\left(\frac{2\bar{v}}{1+v}M^2\sin^2\theta S_2-\sin 2\theta S_3\right)\\ C_{22} &= -(1-M^2\sin^2\theta)\left(\frac{2\bar{v}}{1+v}M^2\sin^2\theta S_1-\cos 2\theta S_3\right) \end{aligned} \tag{17b}$$

$$C_{23}=\frac{3}{2(1+v)}M^2\sin^2\theta g$$

$$\begin{aligned} C_{31} &= M^2\sin^2\theta S_1 g+(1-M^2\sin^2\theta)\sin 2\theta f\\ C_{32} &= M^2\sin^2\theta S_2 g-(1-M^2\sin^2\theta)\cos 2\theta f \end{aligned} \tag{17c}$$

$$C_{33}=\frac{3}{4}M^2\sin^2\theta S_3 g$$

where the functions g and f are defined as:

$$\begin{aligned} g(S_1,S_2) &= -\sin 2\theta S_1+\cos 2\theta S_2\\ f(S_1,S_2,S_3) &= \frac{\sigma_0^3}{nc\mu}3^{-\frac{1+n}{2}}\left[\left(\frac{S_1}{\sigma_0}\right)^2+\left(\frac{S_2}{\sigma_0}\right)^2+\frac{3}{4}\left(\frac{S_3}{\sigma_0}\right)^2\right]^{\frac{3-n}{2}} \end{aligned} \tag{18}$$

Using the coefficient functions $C_{11}\sim C_{33}$ in (17), it can be verified that the determinant of the coefficient matrix $\boldsymbol{C}$ of Eq. (15) has the following form:

$$
\begin{aligned}
&\det C = \frac{3}{2(1+v)} M^4 \sin^4\theta\, g^2 \Delta \\
&\Delta(S_1, S_2, S_3; \theta) = -g^2 + (1 - M^2\sin^2\theta)\big[(1 - 2\bar{v}M^2\sin^2\theta)(S_1^2 + S_2^2) \\
&\qquad + 2(1 - v - \bar{v}M^2\sin^2\theta) f - 2\bar{v}(\cos 2\theta S_1 + \sin 2\theta S_2) S_3 \\
&\qquad + \frac{1}{4}(5 - 4v - 6\bar{v}M^2\sin^2\theta) S_3^2\big]
\end{aligned}
\tag{19}
$$

Due to symmetry, the mode-I crack problem can be discussed only on the upper plane, i.e., $0 \leqslant \theta \leqslant \pi$. From (7), (8), and (13), the boundary conditions for the ordinary differential equations (15) and (16) becomes:

$$
\begin{aligned}
&S_1(0) = -\left(\frac{1}{3}\sigma_{\mathrm{eq}0} - \frac{3}{4}s_{330}\right)^{1/2}, \quad S_2(0) = 0, \quad S_3(0) = s_{330}, \quad v_2(0) = 0, \\
&S_2(\pi) = 0, \quad \sigma_h(\pi) = S_1(\pi)
\end{aligned}
\tag{20}
$$

where $\sigma_{\mathrm{eq}0} = \sigma_{\mathrm{eq}}(0)$, $s_{330} = s_{33}(0)$, both parameters are free unknown constants in the asymptotic analysis, but can be determined from the full-field solutions. In general, the initial equivalent stress $\sigma_{\mathrm{eq}0} \geqslant \sigma_0$ in the plastic zone near the crack tip for a strain hardening material.

3.2. Construction of continuous solutions

If the determinant of the coefficient matrix of equation system (15) equals zero, i.e., $\det \boldsymbol{C} = 0$, then this ordinary differential equation system has non-zero solutions; otherwise, zero solutions only. These two sets of solutions will form the non-constant stress and constant stress sectors in the crack-tip field. Following the solution structure of Zhu and Hwang (2002) for the incompressible hardening materials, we can assemble the dynamic crack-tip field here on the upper half plane using a constant sector in $0 \leqslant \theta \leqslant \theta_1$, a non-constant stress sector in $\theta_1 \leqslant \theta \leqslant \theta_2$, and another constant stress sector in $\theta_2 \leqslant \theta \leqslant \pi$, where θ_1, θ_2 are the sector border angles.

3.2.1. Constant stress sector ① ($0 \leqslant \theta \leqslant \theta_1$)

In the first sector, $\det \boldsymbol{C} \neq 0$, Eqs. (15) and (16) have zero solutions only. Accordingly, all field variables are constants independent of θ. From (15), (16), and (20), we have the constant solutions of deviatoric stresses and particle velocities as:

$$
\begin{aligned}
&s_{11}(\theta) = -\left(\frac{1}{3}\sigma_{\mathrm{eq}0} - \frac{3}{4}s_{330}\right)^{1/2} - \frac{1}{2}s_{330}^2, \qquad s_{12}(\theta) = 0, \qquad s_{33}(\theta) = s_{330} \\
&\sigma_h(\theta) = \sigma_{h0}, \quad \lambda = 0, \quad v_1(\theta) = \mathrm{v}_{10}, \quad \mathrm{v}_2(\theta) = 0
\end{aligned}
\tag{21}
$$

where $\sigma_{h0} = \sigma_h(0)$ is an undetermined constant. The constant v_{10} represents the rigid velocity component in the x_1 direction. For simplicity, $\mathrm{v}_{10} = 0$ is set in this paper. Substitution of (21) into (12) and (13) obtains the components of constant stresses in this sector:

$$
\begin{aligned}
&\sigma_{11}(\theta) = \sigma_{h0} - \left(\frac{1}{3}\sigma_{\mathrm{eq}0} - \frac{3}{4}s_{330}\right)^{1/2} \\
&\sigma_{22}(\theta) = \sigma_{h0} + \left(\frac{1}{3}\sigma_{\mathrm{eq}0} - \frac{3}{4}s_{330}\right)^{1/2} \\
&\sigma_{12}(\theta) = 0 \\
&\sigma_{33}(\theta) = \sigma_{h0} + \frac{3}{2}s_{330}
\end{aligned}
\tag{22}
$$

3.2.2. Non-constant stress sector ② ($\theta_1 \leqslant \theta \leqslant \theta_2$)

In the second sector, $\det \boldsymbol{C} = 0$, Eq. (15) has non-zero solutions and the stress components may be functions of θ. The basic stress variables can be determined using the following equivalent equations of (15):

$$\begin{aligned} &C_{11}S_1'(\theta) + C_{12}S_2'(\theta) + C_{13}S_3'(\theta) = 0 \\ &C_{21}S_1'(\theta) + C_{22}S_2'(\theta) + C_{23}S_3'(\theta) = 0 \\ &\Delta(S_1, S_2, S_3; \theta) = 0 \end{aligned} \tag{23}$$

where Δ is a characteristic function and expressed in (19). The three equations in (23) are the governing equations of the asymptotic solutions that need to be determined in this non-constant stress sector. The other governing equations remain the same as those in (16).

Eq. (23) indicates that the solutions of deviatoric stresses in this non-constant stress sector must stay on the surface of function $\Delta(S_1, S_2, S_3; \theta) = 0$. To solve this equation system, the equation $\Delta(S_1, S_2, S_3; \theta) = 0$ is fully differentiated with respect to S_1, S_2, S_3, and θ, and Eq. (23) becomes

$$\begin{aligned} &C_{11}S_1'(\theta) + C_{12}S_2'(\theta) + C_{13}S_3'(\theta) = 0 \\ &C_{21}S_1'(\theta) + C_{22}S_2'(\theta) + C_{23}S_3'(\theta) = 0 \\ &C_{41}S_1'(\theta) + C_{42}S_2'(\theta) + C_{43}S_3'(\theta) = C_{44} \end{aligned} \tag{24}$$

where the coefficients C_{11}, C_{12}, C_{13}, C_{21}, C_{22}, and C_{23} are the same as those given in (17a) and (17b). The coefficients C_{41}, C_{42}, C_{43}, C_{44} are defined as the first-order partial derivatives of function $\Delta(S_1, S_2, S_3; \theta)$ with respect to S_1, S_2, S_3, and θ, i.e., $C_{41} = \frac{\partial \Delta}{\partial S_1}$, $C_{42} = \frac{\partial \Delta}{\partial S_2}$, $C_{43} = \frac{\partial \Delta}{\partial S_3}$, and $C_{44} = -\frac{\partial \Delta}{\partial \theta}$, and expressed as:

$$\begin{aligned} C_{41} &= \sin 2\theta g + (1 - M_n^2)\left[(1 - 2\bar{\nu}M_n^2)S_1 + (1 - \nu - \bar{\nu}M_n^2)\frac{\partial f}{\partial S_1} - \bar{\nu}\cos 2\theta S_3\right] \\ C_{42} &= -\cos 2\theta g + (1 - M_n^2)\left[(1 - 2\bar{\nu}M_n^2)S_2 + (1 - \nu - \bar{\nu}M_n^2)\frac{\partial f}{\partial S_2} - \bar{\nu}\sin 2\theta S_3\right] \\ C_{43} &= (1 - M_n^2)\left[(1 - \nu - \bar{\nu}M_n^2)\frac{\partial f}{\partial S_1} - \bar{\nu}(\cos 2\theta S_1 + \sin 2\theta S_2) + \frac{1}{4}(5 - 4\nu - 6\bar{\nu}M_n^2)S_3\right] \\ C_{44} &= -2(\cos 2\theta S_1 + \sin 2\theta S_2)g + 2\bar{\nu}(1 - M_n^2)\left[M_n^2 \cot\theta(S_1^2 + S_2^2 + \frac{3}{4}S_3^2 + f) + gS_3\right] \\ &\quad + M_n^2 \cot\theta\left[(1 - 2\bar{\nu}M_n^2)(.S_1^2 + S_2^2) + 2(1 - \nu - \bar{\nu}M_n^2)f\right. \\ &\quad \left. - 2\bar{\nu}(\cos 2\theta S_1 + \sin 2\theta S_2)S_3 + \frac{1}{4}(5 - 4\nu - 6\bar{\nu}M_n^2)S_3^2\right] \end{aligned} \tag{25}$$

where $M_n = M\sin\theta$ and the three partial derivatives of function f are:

$$\begin{aligned} \frac{\partial f}{\partial S_1} &= \frac{(3-n)\sigma_0}{nc\mu} 3^{-\frac{1+n}{2}} S_1 \left[\left(\frac{S_1}{\sigma_0}\right)^2 + \left(\frac{S_2}{\sigma_0}\right)^2 + \frac{3}{4}\left(\frac{S_3}{\sigma_0}\right)^2\right]^{\frac{1-n}{2}} \\ \frac{\partial f}{\partial S_2} &= \frac{(3-n)\sigma_0}{nc\mu} 3^{-\frac{1+n}{2}} S_2 \left[\left(\frac{S_1}{\sigma_0}\right)^2 + \left(\frac{S_2}{\sigma_0}\right)^2 + \frac{3}{4}\left(\frac{S_3}{\sigma_0}\right)^2\right]^{\frac{1-n}{2}} \\ \frac{\partial f}{\partial S_3} &= \frac{3(3-n)\sigma_0}{4nc\mu} 3^{-\frac{1+n}{2}} S_3 \left[\left(\frac{S_1}{\sigma_0}\right)^2 + \left(\frac{S_2}{\sigma_0}\right)^2 + \frac{3}{4}\left(\frac{S_3}{\sigma_0}\right)^2\right]^{\frac{1-n}{2}} \end{aligned} \tag{26}$$

Through solving (24), one obtains:

$$
\begin{aligned}
S_1'(\theta) &= \frac{C_{44}}{J}(C_{12}C_{23} - C_{13}C_{22}) \\
S_2'(\theta) &= \frac{C_{44}}{J}(C_{13}C_{21} - C_{11}C_{23}) \\
S_3'(\theta) &= \frac{C_{44}}{J}(C_{11}C_{22} - C_{12}C_{21})
\end{aligned}
\tag{27}
$$

where J is the determinant of the coefficient matrix of Eq. (24), and expressed as:

$$
J = C_{11}C_{22}C_{43} + C_{21}C_{42}C_{23} + C_{41}C_{23}C_{12} - C_{13}C_{22}C_{41} - C_{23}C_{42}C_{11} - C_{43}C_{21}C_{12} \tag{28}
$$

Accordingly, the deviatoric stress components in this sector can be directly determined by integrating Eq. (27), and then the in-plane mean stress and the particle velocities are determined by integrating Eq. (16) from the sector angle $\theta = \theta_1$ to θ_2.

3.2.3. Constant stress sector ③ ($\theta_2 \leqslant \theta \leqslant \pi$)

In this third sector, $\det \boldsymbol{C} \neq 0$. Again, all field variables are constant and obtained as:

$$
\begin{aligned}
&s_{11}(\theta) = s_{11\pi}, \quad s_{12}(\theta) = 0, \quad s_{33}(\theta) = s_{33\pi} \\
&\sigma_h(\theta) = s_{11\pi} + s_{33\pi}/2, \quad \lambda = 0, \quad \mathrm{v}_1(\theta) = \mathrm{v}_{1\pi}, \quad \mathrm{v}_2(\theta) = \mathrm{v}_{2\pi}
\end{aligned}
\tag{29}
$$

where $s_{11\pi} = s_{11}(\pi)$, $s_{33\pi} = s_{33}(\pi)$, $\mathrm{v}_{1\pi} = \mathrm{v}_1(\pi)$, and $\mathrm{v}_{2\pi} = \mathrm{v}_2(\pi)$ are undetermined constants. Substituting (29) into (12) and (13) obtains the constant stresses components in this sector:

$$
\begin{aligned}
\sigma_{11}(\theta) &= 2s_{11\pi} + s_{33\pi} \\
\sigma_{22}(\theta) &= 0 \\
\sigma_{12}(\theta) &= 0 \\
\sigma_{33}(\theta) &= s_{11\pi} + 2s_{33\pi}
\end{aligned}
\tag{30}
$$

3.3. Determination of sector border angles

The continuity condition (9) requires that all stresses, strains, and particle velocities are continuous at the sector connections where $\theta = \theta_1$ and $\theta = \theta_2$. At these sector border angles, the constant solutions in (21) and (29) specify the boundary conditions for the asymptotic governing equations (27) and (16) in the sector ② as:

$$
\begin{aligned}
&S_1(\theta_1) = -\left[\frac{1}{3}\sigma_{\mathrm{eq}0}^2 - \frac{3}{4}s_{330}^2\right]^{1/2}, \qquad S_2(\theta_1) = 0, \qquad S_3(\theta_1) = s_{330} \\
&\sigma_h(\theta_1) = \sigma_{h0}, \quad \mathrm{v}_1(\theta_1) = 0, \quad \mathrm{v}_2(\theta_1) = 0
\end{aligned}
\tag{31}
$$

and

$$
\begin{aligned}
&S_1(\theta_2) = s_{11\pi} + s_{33\pi}/2, \quad S_2(\theta_2) = 0, \quad S_3(\theta_2) = s_{33\pi} \\
&\sigma_h(\theta_2) = s_{11\pi} + s_{33\pi}/2, \quad \mathrm{v}_1(\theta_2) = \mathrm{v}_{1\pi}, \quad \mathrm{v}_2(\theta_2) = \mathrm{v}_{2\pi}
\end{aligned}
\tag{32}
$$

According to (23), the initial boundary point of stresses at $\theta = \theta_1$ must lie on the characteristic surface defined by $\Delta(S_1, S_2, S_3; \theta) = 0$. Because there are two initial unknown parameters, $\sigma_{\mathrm{eq}0}$ and s_{330}, it is generally difficult to determine the sector border angle θ_1. However, if the initial equivalent stress $\sigma_{\mathrm{eq}0}$ is given, the values of s_{330} and θ_1 can be solved from the following equations:

$$
\begin{aligned}
&\Delta(S_1(\theta_1), 0, s_{330}; \theta_1) = 0 \\
&C_{44}(S_1(\theta_1), 0, s_{330}; \theta_1) = 0 \\
&S_1(\theta_1) = -\left[\frac{1}{3}\sigma_{\mathrm{eq}0}^2 - \frac{3}{4}s_{330}^2\right]^{1/2}
\end{aligned}
\tag{33}
$$

Solving the nonlinear equation system in (33) may give two ultimate values of s_{330}, namely the maximum value $s_{330\max}$ and the minimum value $s_{330\min}$, and the corresponding border angle θ_1. The other border angle θ_2 can be determined as the condition $S_2(\theta_2) = 0$ is met during the integration of Eq. (27). Note that if a full-field solution is known, the two parameters σ_{eq0} and s_{330} can be determined by matching the asymptotic solution in (22) with the full-field stresses at $\theta = 0$, and then the sector border angle θ_1 can be solved from the first equation in (33) only.

From the analysis above, one knows that the fully continuous solution near the dynamically propagating crack tip contains two free parameters, σ_{eq0} and s_{330}, and thus constitutes a two-parameter family of solutions.

3.4. Approximate behavior of the present solutions as $\nu \to 0.5$

When the Poisson ratio $\nu \to 0.5$, a compressive hardening material approaches an incompressible hardening material, and thus the present solutions are anticipated to reduce to those for incompressible power-law materials (Zhu and Hwang, 2002). As $\nu \to 0.5$ or $\bar{\nu} \to 0$, from the plane strain condition (6), one has $s_{33} = 0$ at the crack tip. And then from (17a), (18), and (19), we have:

$$C_{11} = -\frac{1}{2}\sin 4\theta s_{11} - (\sin^2 2\theta - M^2 \sin^2\theta)s_{12} \tag{34}$$

$$C_{12} = \frac{1}{2}\sin 4\theta s_{12} + (\cos^2 2\theta - M^2 \sin^2\theta)s_{11}$$

$$\Delta(s_{11}, s_{12}; \theta) = (\cos 2\theta s_{11} + \sin 2\theta s_{12})^2 - M^2 \sin^2\theta \lfloor s_{11}^2 + s_{12}^2 + f \rfloor + f \tag{35}$$

$$f(s_{11}, s_{12}) = \frac{\sigma_0^3}{nc\mu} 3^{-\frac{1+n}{2}} \left[\left(\frac{s_{11}}{\sigma_0}\right)^2 + \left(\frac{s_{12}}{\sigma_0}\right)^2 \right]^{\frac{3-n}{2}} \tag{36}$$

Moreover, it is verified that the second equation in (23) holds automatically, and thus the asymptotic governing (23) is simplified as:

$$\begin{aligned} &C_{11}s'_{11}(\theta) + C_{12}s'_{12}(\theta) = 0 \\ &\Delta(s_{11}, s_{12}; \theta) = 0 \end{aligned} \tag{37}$$

and the equations in (16) are simplified as:

$$\begin{aligned} &\sigma'_h(\theta) = \cos 2\theta s'_{11}(\theta) + \sin 2\theta s'_{12}(\theta) \\ &\lambda = -\frac{V \sin\theta}{2\mu r} \cdot \frac{\cos 2\theta s'_{11}(\theta) + \sin 2\theta s'_{12}(\theta)}{\cos 2\theta s_{11}(\theta) + \sin 2\theta s_{12}(\theta)} \\ &v'_1(\theta) = \frac{V \cot\theta}{\mu M^2}\left[\cos 2\theta s'_{12}(\theta) - \sin 2\theta s'_{11}(\theta)\right] \\ &v'_2(\theta) = \frac{V}{\mu M^2}\left[\cos 2\theta s'_{12}(\theta) - \sin 2\theta s'_{11}(\theta)\right] \end{aligned} \tag{38}$$

Through comparisons, it is found that (37) and (38) are the same as the asymptotic governing (22) and (17) in the non-constant stress sector that were given by Zhu and Hwang (2002) for the incompressible hardening materials. Further analysis shows that for $\nu \to 0.5$, the solutions (21) and (32) in the first and third constant stress sectors are also the same as those given by Zhu and Hwang (2002). As a result, it is concluded that the present solutions for compressible hardening materials can reduce to those developed by Zhu and Hwang (2002) for the incompressible hardening materials in the limit of $\nu \to 0.5$.

3.5. Approximate behavior of the present solutions as $n \to \infty$

As similar to the discussions above, the approximate behavior of the present solutions can analyzed for $n \to \infty$. When the hardening exponent $n \to \infty$, the hardening material approaches the elastic–perfectly plastic material. It is anticipated that the present solutions can reduce to those proposed by Zhang et al. (1997). In

fact, when n goes infinity, the Mises equivalent stress σ_{eq} approaches the yield stress σ_0 in plastic regions. Thus from (14), the three deviatoric stress components can be expressed by:

$$\begin{aligned} S_1 &= -k\cos\phi(\theta)\cos(\psi(\theta)-2\theta) \\ S_2 &= k\cos\phi(\theta)\sin(\psi(\theta)-2\theta) \\ S_3 &= -\frac{2}{\sqrt{3}}\sin\phi(\theta) \end{aligned} \tag{39}$$

where $k=\sigma_0/\sqrt{3}$ is the shear yield strength, $\psi(\theta)$, and $\phi(\theta)$ are the stress functions of θ, and independent of n. As $n\to\infty$, it is found that $f\to 0$ in (19) and the asymptotic governing (33) and (16) in the second sector can reduce to Eqs. (3.15) and (3.5) given by Zhang et al. (1997) for the compressible elastic–perfectly plastic materials. Moreover, the solutions (21) and (32) in the first and third sectors reduce to the corresponding ones given by Zhang et al. (1997). Therefore, the present solutions for the compressive hardening materials can reduce to those developed by Zhang et al. (1997) for the compressive elastic–perfectly plastic materials in the limit of $n\to\infty$.

4. Numerical integrations and result analyses

4.1. Crack-tip stress fields

For a specific hardening exponent n, a Poisson ratio v, and a crack growth speed M, the three ordinary differential equations in (27) can be solved under the boundary conditions in (31) using a numerical integration method. However, the numerical integration depends on the initial equivalent stress σ_{eq0}, the initial deviatoric stress s_{330} and the material constant ratio $\sigma_0/c\mu$. The hardening relation (4) shows that the material constants c and σ_0 are dependent on each other. Without loss of generality, we choose $\sigma_0/c\mu=1$ in the numerical integration. The strategy for numerical integrations of (27) used in this work is outlined as follows:

(1) For the given values of σ_{eq0}, n, v, and M, two ultimate values of s_{330}, i.e., s_{330max} and s_{330min}, and the corresponding sector border angle θ_1 can be determined by solving the nonlinear equation system (33). At $\theta=\theta_1$, the boundary conditions for the ordinary differential equations in (27) are specified by the first three stress equations of (31).
(2) Using the fourth-order Runge–Kutta method, the differential equation system (27) in sector ② is numerically integrated forward starting from θ_1 and ending at θ_2, where the boundary condition $S_2(\theta_2)=0$ is satisfied. Accordingly, the variables $S_1(\theta)$, $S_2(\theta)$, and $S_3(\theta)$ are determined. Using the relation in (12), the deviatoric stress components $s_{11}(\theta)$, $s_{12}(\theta)$, and $s_{33}(\theta)$ in the non-constant stress sector ② are then determined. Moreover, at the sector border angle $\theta=\theta_2$, the deviatoric stress constants are obtained as $s_{11\pi}=s_{11}(\theta_2)$ and $s_{33\pi}=s_{33}(\theta_2)$.
(3) With the functions of $S_1(\theta)$, $S_2(\theta)$, and $S_3(\theta)$ known, the in-plane mean stress $\sigma_h(\theta)$ in sector ② is determined under the boundary condition $\sigma_h(\theta_2)=s_{11\pi}+s_{33\pi}/2$ as specified in (32) through the backward integration of the first differential equation of (16) from θ_2 to θ_1. Then the hydrostatic stress constant is obtained as $\sigma_{h0}=\sigma_h(\theta_1)$.
(4) In the constant stress sector ① and sector ③, all components of deviatoric stresses and in-plane mean stress can be obtained from those in sector ② at the two sector angles with consideration of the continuity condition (9).
(5) All stress components over the entire angles around the crack tip can be finally determined from (13).

It should be noted that for a known full-field solution, such as a finite element solution for a dynamic crack, the step (1) above becomes to determine the two parameters σ_{eq0} and s_{330} by matching the asymptotic stress solutions in (22) with those extracted from the full-field solution at $\theta=0$, and then to determine the sector border angle θ_1 by solving the first equation in (33) only. With the value of θ_1, the same procedures stated in steps (2)–(5) can be followed to determine all stress components for the asymptotic crack-tip field. However, such analysis cannot be further demonstrated without a full-field solution for a dynamic crack.

Let's focus on the asymptotic crack-tip field only hereafter. If the values of the initial equivalent stress σ_{eq0}, the strain hardening exponent n, the Poisson ratio v, and the Mach number M are specified, the fully continuous angular variations of stresses can be determined using the numerical integration strategy stated above. Figs. 1 and 2 show the effects of n and v on the angular variations of the deviatoric stress components $s_{11}(\theta)$, $s_{12}(\theta)$, and $s_{33}(\theta)$, respectively, for $\sigma_{eq0} = 1$, $n = 3$, $v = 0.3$, $M = 0.5$ and the resulted values of s_{330max}, s_{330min}, and θ_1. Noted that the value of σ_{eq0} used in all plots of this paper are normalized by the yield stress σ_0. The values of s_{330max}, s_{330min}, and θ_1 can be found easily from Fig. 1(b) or Fig. 2(b). Comparing to the strain hardening exponent n, these two figures indicate that the Poisson ratio has relatively small effects on the deviatoric stress components in the asymptotic crack-tip field.

With the deviatoric stress components, all stress components $\sigma_{11}(\theta)$, $\sigma_{22}(\theta)$, $\sigma_{12}(\theta)$, $\sigma_{33}(\theta)$, and $\sigma_{eq}(\theta)$ at the dynamic crack tip can be easily determined. Fig. 3 displays the effect of the initial deviatoric stress s_{330} on the stress field for $\sigma_{eq0} = 1$, $n = 3$, $v = 0.3$, and $M = 0.5$. It is evident from this figure that s_{330} has no notable effect on the in-plane stress components and the Mises equivalent stress, and only some effect on the out-plane stress σ_{33}. Accordingly, s_{330max} is used only hereafter for all followed analyses. Fig. 4 plots the stress field for three different initial equivalent stresses: $\sigma_{eq0} = 1.0$, 1.5, and 2.0 with $n = 3$, $v = 0.3$, and $M = 0.5$, respectively.

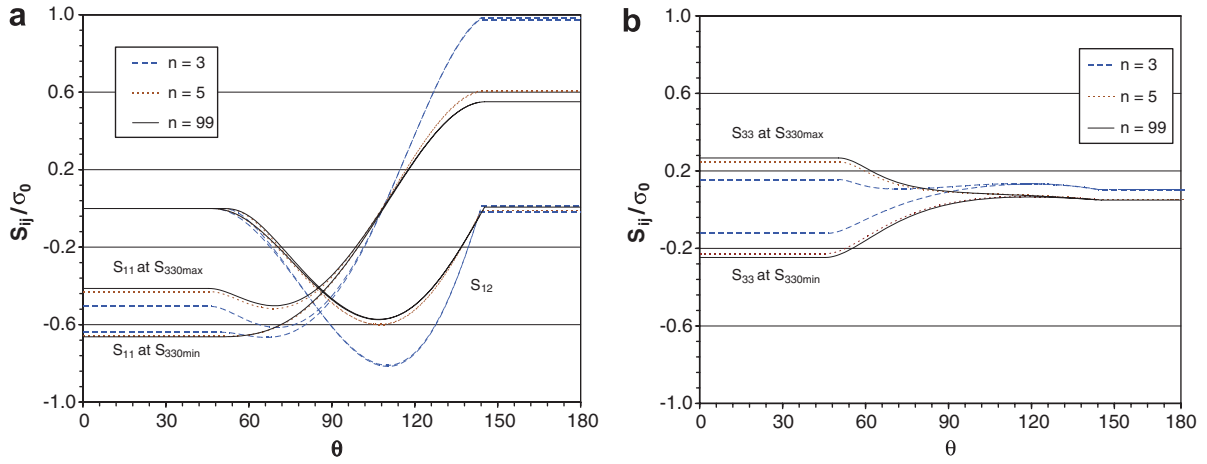

Fig. 1. Angular variations of deviatoric stress components for $n = 3$, 5, and 99 with $\sigma_{eq0} = 1$, $v = 0.3$, and $M = 0.5$. (a) In-plane deviatoric stress S_{11} and S_{12}; (b) out-plane deviatoric stress S_{33}.

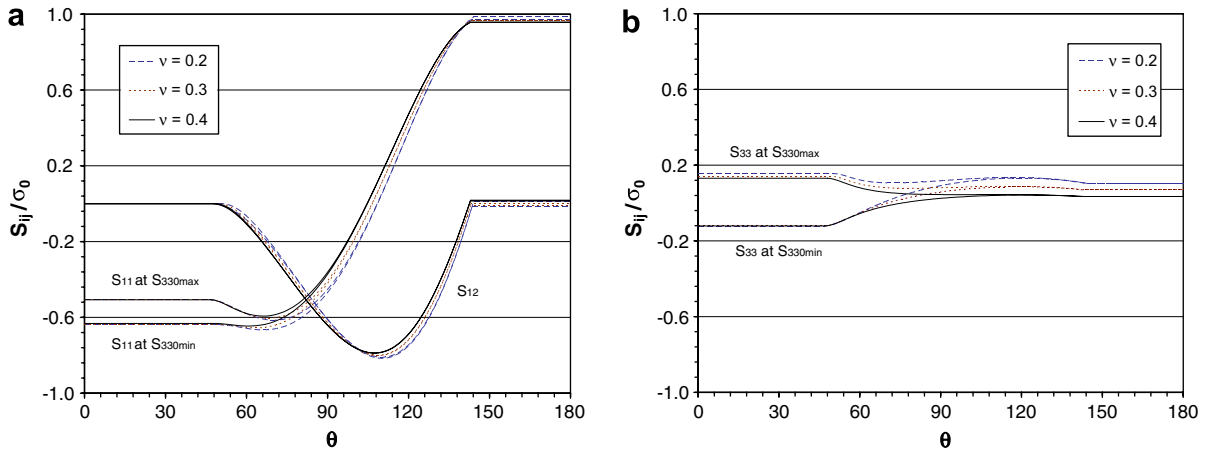

Fig. 2. Angular variations of deviatoric stress components for $v = 0.2$, 0.3, and 0.4 with $\sigma_{eq0} = 1$, $n = 3$, and $M = 0.5$. (a) In-plane deviatoric stress S_{11} and S_{12}; (b) out-plane deviatoric stress S_{33}.

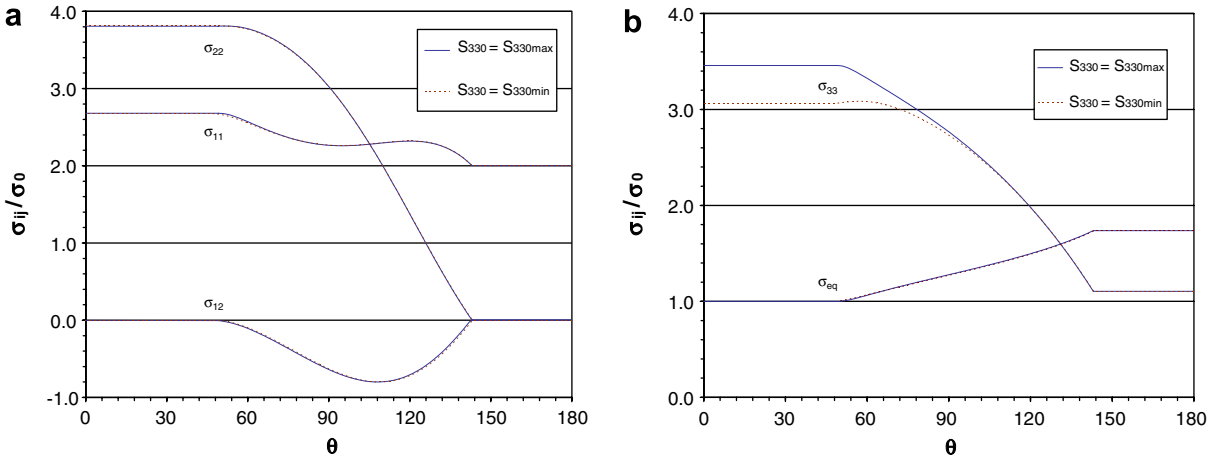

Fig. 3. Effect of the initial deviatoric stress ε_{330} on the angular variations of stress components for $\sigma_{eq0} = 1$, $n = 3$, $v = 0.3$, and $M = 0.5$. (a) In-plane stress components σ_{11}, σ_{12}, and σ_{22}; (b) out-plane stress σ_{33}, and equivalent stress σ_{eq}.

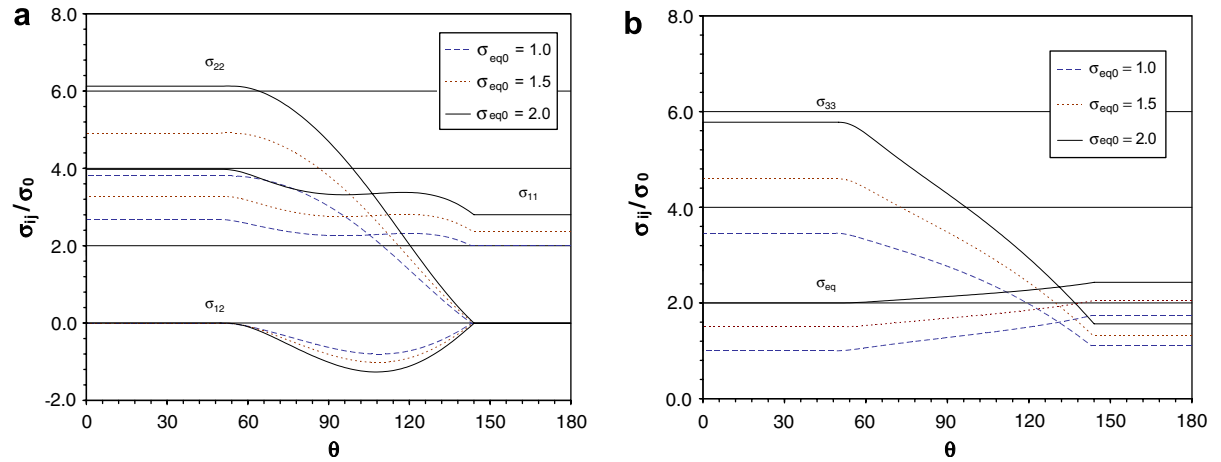

Fig. 4. Effect of the initial equivalent stress σ_{eq0} on the angular variations of stress components for $n = 3$, $v = 0.3$, and $M = 0.5$. (a) In-plane stress components σ_{11}, σ_{12}, and σ_{22}; (b) out-plane stress σ_{33}, and equivalent stress σ_{eq}.

Unlike to the initial deviatoric stress s_{330}, Fig. 4 shows the initial equivalent stress σ_{eq0} has very strong effect on all stress components in the asymptotic crack-tip field.

Fig. 5 depicts the angular variations of all stress components for three strain hardening exponent: $n = 3$, 5, and 99 with $\sigma_{eq0} = 1$, $v = 0.3$, and $M = 0.5$, respectively. Note that $n = 99$ is intended to approximate the non-hardening material. This figure indicates that the results of stresses for the intermediate hardening material with $n = 5$ are very close to those for the low hardening material with $n = 99$, but significantly different from those for the high hardening material with $n = 3$. Through comparison, it is found that the stress field for the low hardening exponent $n = 99$ is almost identical to that obtained by Zhang et al. (1997) for the compressible elastic–perfectly plastic materials. This verifies our previous conclusion that the present solution reduces to that for the corresponding elastic–perfectly plastic material in the limit of $n \to \infty$.

Fig. 6 plots the angular variations of the stress components for three Poisson ratios: $v = 0.2$, 0.3, and 0.4 with $\sigma_{eq0} = 1$, $n = 3$, and $M = 0.5$, respectively. The results of stresses for $v = 0.5$ obtained in Zhu and Hwang (2002) for incompressible hardening materials are also included in Fig. 6. This figure shows that the Poisson ratio has certain effect on the dynamic crack-tip stress field, and all stress components approaches those for $v = 0.5$. This confirms our previous finding that the present solution reduces to that for the incompressible hardening materials in the limit of $v \to 0.5$.

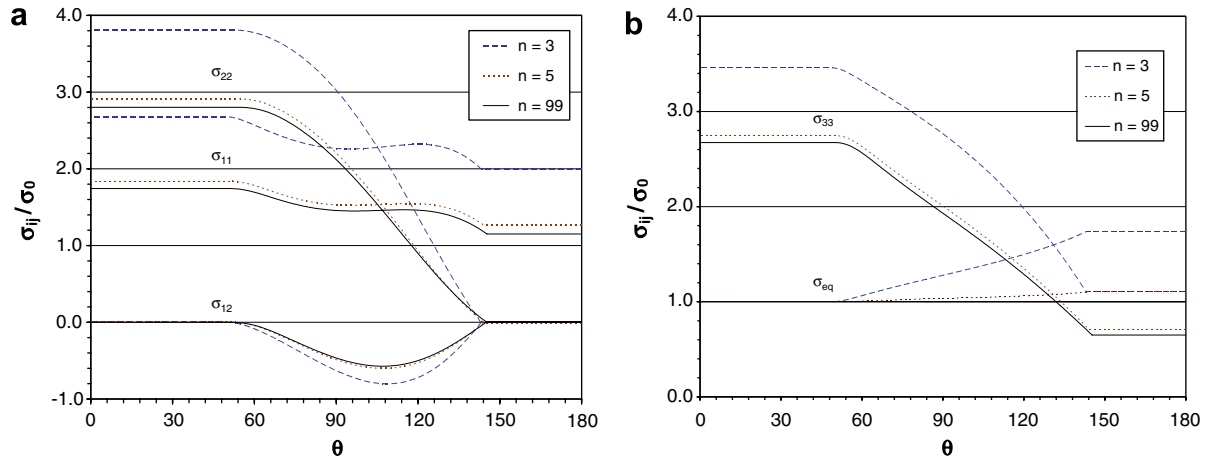

Fig. 5. Effect of the strain hardening exponent n on the angular variations of stress components for $\sigma_{eq0} = 1$, $v = 0.3$, and $M = 0.5$. (a) In-plane stress components σ_{11}, σ_{12}, and σ_{22}; (b) out-plane stress σ_{33}, and equivalent stress σ_{eq}.

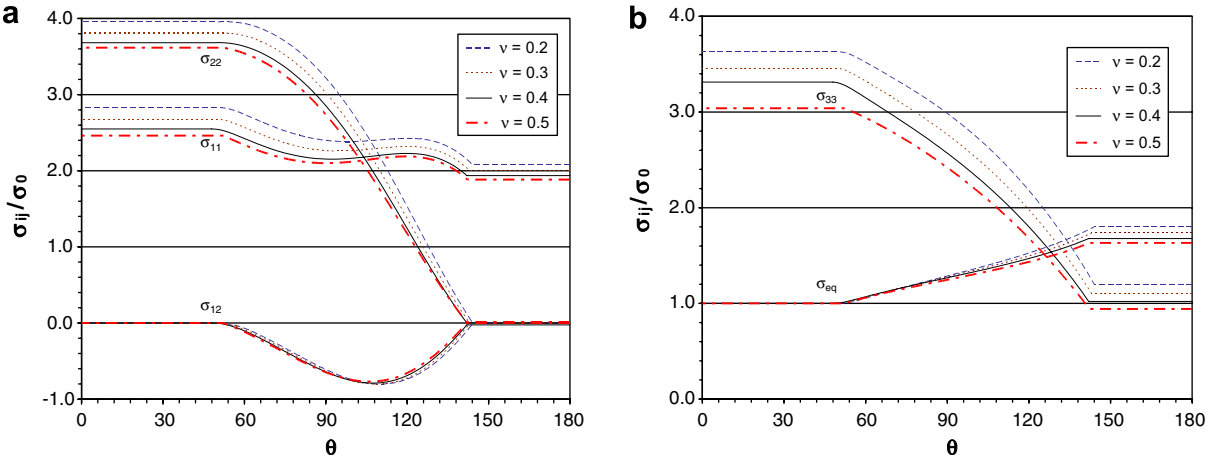

Fig. 6. Effect of the Poisson ratio v on the angular variations of stress components for $\sigma_{eq0} = 1$, $n = 3$, and $M = 0.5$. (a) In-plane stress components σ_{11}, σ_{12}, and σ_{22}; (b) out-plane stress σ_{33}, and equivalent stress σ_{eq}.

Fig. 7 shows the stress field for three Mach number $M = 0.3$, 0.5, and 0.8 with $\sigma_{eq0} = 1$, $n = 8$, and $v = 0.4$, respectively. As evident from this figure, the Mach number M has significant effect on the asymptotic stress field. As a summary, from Figs. 3–7, it is observed that (a) the parameter s_{330} has some effect only for the out-plane stress, (b) the Poisson ratio has intermediate effect on the stress field, (c) all other three parameters σ_{eq0}, n, and M have significant effects on the stress field, (d) all three normal stresses and thus the hydrostatic stress increase or decrease as the parameters n, v, or M decreases or increases. For all cases considered, it is seen that the stress fields are fully continuous, and $\sigma_{eq}(\theta) \geqslant \sigma_{eq0} \geqslant \sigma_0$ around the crack tip. As a result, no elastic unloading occurs near the crack surfaces in the present solution.

4.2. Velocity and strain fields

With the functions of $S_1(\theta)$, $S_2(\theta)$, and $\sigma_h(\theta)$ determined above from (27), the components of particle velocity and strain tensor can be obtained by integrating the last two equations of (16) and the geometrical relation (2), respectively, along a line $x_2 = constant$. In sector ②, using the velocity boundary conditions as specified by the last two equations in (31), we have the particle velocity and strain components as:

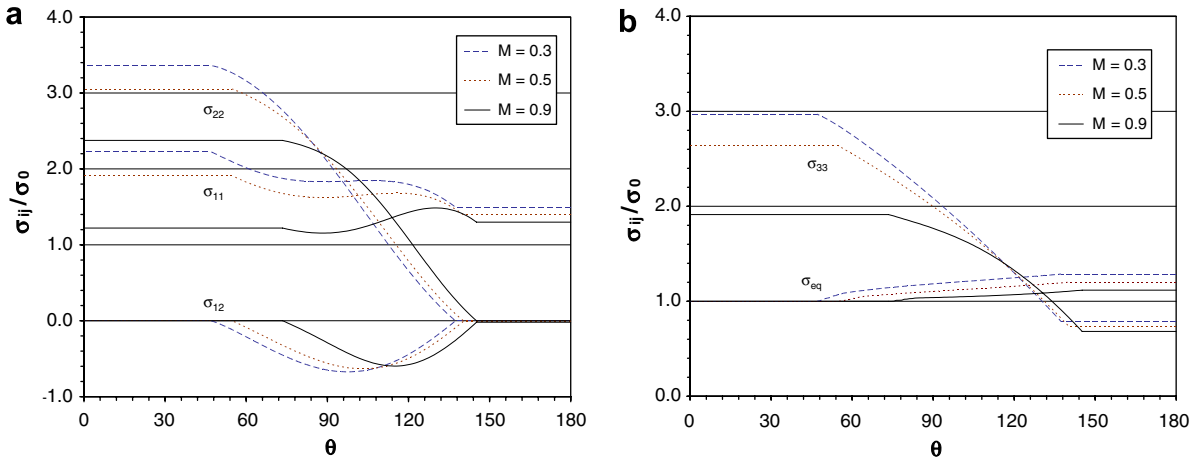

Fig. 7. Effect of the Mach number M on the angular variations of stress components for $\sigma_{eq0} = 1$, $n = 8$, and $v = 0.4$. (a) In-plane stress components σ_{11}, σ_{12}, and σ_{22}; (b) out-plane stress σ_{33}, and equivalent stress σ_{eq}.

$$\begin{aligned} \mathrm{v}_1(\theta) &= -\frac{V}{\mu M^2}\int_{\theta_1}^{\theta}[(S_1'(\theta)+\sigma_h'(\theta)) - \cot\theta S_2'(\theta)]\mathrm{d}\theta \\ \mathrm{v}_2(\theta) &= -\frac{V}{\mu M^2}\int_{\theta_1}^{\theta}[\cot\theta(S_1'(\theta)-\sigma_h'(\theta)) + S_2'(\theta)]\mathrm{d}\theta \end{aligned} \tag{40}$$

and

$$\begin{aligned} \varepsilon_{11}(\theta) &= -\frac{1}{V}\mathrm{v}_1(\theta) \\ \varepsilon_{22} &= \varepsilon_{220} - \frac{1}{\mu M^2}\int_{\theta_1}^{\theta}\cot\theta[\cot\theta(S_1'(\theta)-\sigma_h'(\theta)) + S_2'(\theta)]\mathrm{d}\theta \\ \varepsilon_{12}(\theta) &= \frac{1}{2\mu M^2}\int_{\theta_1}^{\theta}\frac{1}{\sin^2\theta}[S_2'(\theta) - \sin 2\theta\,\sigma_h'(\theta)]\mathrm{d}\theta \end{aligned} \tag{41}$$

where ε_{220} is an integration constant that can only be determined by matching the present solution to the full-field solution. The particle velocity and strain components are uniform in sectors ① and ③. The uniform values can be determined by (40) and (41) with consideration of the continuity condition (9).

Fig. 8(a) shows the angular variations of particle velocities for three hardening exponents $n = 3$, 5, and 99 with $\sigma_{eq0} = 1$, $v = 0.3$, and $M = 0.5$, respectively. Fig. 8(b) displays the angular distributions of particle velocities for three Poisson ratios $v = 0.2$, 0.3, 0.4 with $\sigma_{eq0} = 1$, $n = 3$, and $M = 0.5$, respectively. Fig. 9(a) shows the angular variations of three strain components for three hardening exponents $n = 3$, 5, and 99 with $\sigma_{eq0} = 1$, $v = 0.3$, and $M = 0.5$, respectively. Fig. 9(b) displays the angular distributions of three strain components for three Poisson ratios $v = 0.2$, 0.3, 0.4 with $\sigma_{eq0} = 1$, $n = 3$, and $M = 0.5$, respectively. It is noted that the unknown constant ε_{220} has been arbitrarily chosen as $\varepsilon_{220} = 1.0$ in Fig. 9 for demonstrating the strain variations. From Figs. 8 and 9, it is observed that both hardening exponent n and the Poisson ratio v have significant effects on the asymptotic deformation fields including velocity and strain fields at the dynamically propagating crack tip. Similar influences on the crack-tip deformation fields are found for the initial equivalent stress σ_{eq0} and the Mach number M, which are not shown here due to space limitation.

5. Conclusions

The present paper extends our previous work (Zhu and Hwang, 2002) for the incompressible hardening materials to the compressible power-law hardening material so as to study the effects of material compressibil-

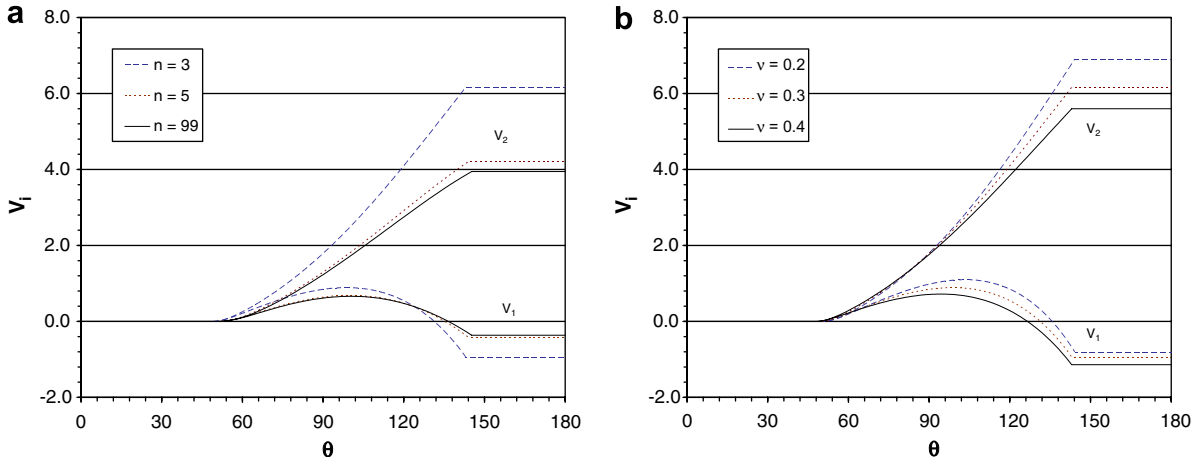

Fig. 8. Angular variations of particle velocities. (a) $n = 3$, 5, and 99 for $\sigma_{eq0} = 1$, $v = 0.3$, and $M = 0.5$; (b) $v = 0.2$, 0.3, and 0.4 for $\sigma_{eq0} = 1$, $n = 3$, and $M = 0.5$.

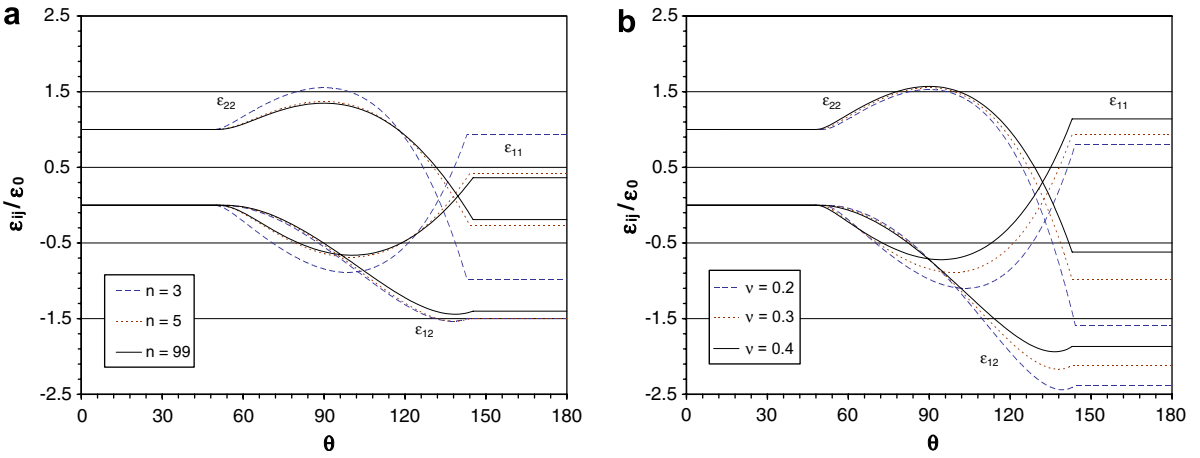

Fig. 9. Angular variations of stress components at $\varepsilon_{220} = 1.0$. (a) $n = 3$, 5, and 99 for $\sigma_{eq0} = 1$, $v = 0.3$, and $M = 0.5$; (b) $v = 0.2$, 0.3, and 0.4 for $\sigma_{eq0} = 1$, $n = 3$, and $M = 0.5$.

ity on asymptotic fields for mode-I dynamic cracks. Our attention is focused on constructing fully continuous asymptotic stress and strain fields under the plane strain condition. Primary results are summarized as follows:

(1) In terms of the assumption that the stresses, strains, and particle velocities at the crack tip are bounded, the fully continuous stress and deformation fields are constructed for the mode-I dynamic cracks. There are two free parameters σ_{eq0} and s_{330} in the proposed asymptotic fields, and they can be determined from the full-field solutions.

(2) Both crack-tip stress and deformation fields are affected significantly by the initial equivalent stress σ_{eq0}, the hardening exponent n, the Poisson ratio v, and the Mach number M, but not by the initial deviatoric stress s_{330}. Both the crack-opening stress and the hydrostatic stress (i.e., stress triaxiality) ahead of the crack tip decrease (or increase) as n, v, or M increases (or decreases).

(3) In the limit as the hardening exponent goes to infinity or $n \to \infty$, the free parameter σ_{eq0} approaches the yield stress σ_0 and the present solutions approach those of Zhang et al. (1997) for the compressible elastic–perfectly plastic materials.

(4) In the limit as the Poisson ratio goes to 0.5, i.e., $v \to 0.5$, the present solutions approach those of Zhu and Hwang (2002) for the incompressible power-law hardening materials.

(5) In the proposed continuous solutions, the crack-tip fields are entirely comprised of plastic sectors, and there is no elastic unloading zone near the crack surfaces. In this regard, the present solutions cannot reduce to those for the quasi-static growth crack in the limit of vanishing crack speed, and are inconsistent with available FEA or EFG results for the dynamic cracks. Therefore, further theoretical, numerical, or experimental investigations of the crack-tip fields for the steady dynamic cracks are needed so as to better understand the mechanics behaviors of dynamic crack-tip fields.

Acknowledgments

The present work is prepared based on the Ph.D. dissertation of Zhu (1995) that was partly supported by the National Natural Science Foundation of China through Cooperative Agreement No. 19392300. Helpful discussions with Dr. Lin Zhang are greatly appreciated.

References

Drugan, W.J., Shen, Y., 1987. Restrictions on dynamically propagating surfaces of strong discontinuity in elastic–plastic solids. Journal of the Mechanics and Physics of Solids 35, 771–787.

Freund, L.B., 1998. Dynamic Fracture Mechanics. Cambridge University Press, Cambridge, United Kingdom.

Gao, Y.C., 1985. Asymptotic dynamic solution to the mode-I propagating crack-tip filed. International Journal of Fracture 29, 171–180.

Gao, Y.C., Nemat-Nasser, S., 1983a. Dynamic fields near a crack tip growing in an elastic–perfectly plastic solid. Mechanics of Materials 2, 47–60.

Gao, Y.C., Nemat-Nasser, S., 1983b. Near tip dynamic fields for a crack advancing in a power law elastic–plastic material: modes I, II and III. Mechanics of Materials 2, 305–317.

Lam, P.S., Freund, L.B., 1985. Analysis of dynamic growth of a tensile crack in an elastic–plastic material. Journal of the Mechanics and Physics of Solids 33, 153–167.

Leighton, J.T., Champion, C.R., Freund, L.B., 1987. Asymptotic analysis of steady dynamic crack growth in an elastic–plastic material. Journal of the Mechanics and Physics of Solids 35, 541–563.

Rosakis, A.J., Ravichandran, G., 2000. Dynamic failure mechanics. International Journal of Solids and Structures 37, 331–348.

Varias, A.G., Shih, C.F., 1994. Dynamic steady crack growth in elastic–plastic solids—propagation of strong discontinuities. Journal of the Mechanics and Physics of Solids 42, 1817–1848.

Wall, O., 2002. Numerical modeling of fracture initiation in large steel specimens at impact. Engineering Fracture Mechanics 69, 851–856.

Xu, Y., Saigal, S., 1999. An element free Galerkin analysis of steady dynamic growth of a model I crack in elastic–plastic materials. International of Journal of Solids and Structures 36, 1045–1079.

Zhang, X., Qin, Q.H., Mai, Y.W., 2003. Asymptotic fields for dynamic crack growth in non-associative pressure sensitive materials. International Journal of Solids and Structures 40, 649–670.

Zhang, L., Zhu, X.K., Hwang, K.C., 1997. Near-tip fields of steady dynamic crack growth in a compressible elastic–plastic material. Journal of the Mechanics of Physics and Solids 45, 989–1005.

Zhu, X.K., 1995. Research on the dynamic near-tip fields in elastic–plastic materials, Ph.D. dissertation, Tsinghua University, Beijing, China.

Zhu, X.K., Hwang, K.C., 1996. Dynamic asymptotic fields near a crack tip growing in a power-law hardening compressible material. Mechanics of Material 24, 213–220.

Zhu, X.K., Hwang, K.C., 2002. Dynamic crack-tip field for tensile cracks propagating in power-law hardening materials. International Journal of Fracture 115, 323–342.